SSRG International Journal of Electrical and Electronics Engineering
ISSN: 2348-8379/ https://doi.org/10.14445/23488379/IJEEE-V11I10P108

Volume 11 Issue 10, 71-82, October 2024

Original Article

Design and Validation of a 6-Port Planar MIMO Array for Sub-6 GHz 5G Bands

A.K.M. Zakir Hossain[1*], Muhammad Ibn Ibrahimy[2], Mohd Khanapiah Bin Nor[1], Abdul Halim Bin Dahalan[1]

[1]*Centre for Telecommunication Research & Innovation (CeTRI), Fakulti Teknologi dan Kejeruteraan Elektronik dan Komputer (FTKEK), Universiti Teknikal Malaysia Melaka (UTeM), Melaka, Malaysia.*
[2]*Department of Electrical and Computer Engineering, Faculty of Engineering, International Islamic University Malaysia, Gombak, Malaysia.*

**Corresponding Author : zakir@utem.edu.my*

Received: 05 August 2024 Revised: 06 September 2024 Accepted: 07 October 2024 Published: 30 October 2024

Abstract *- This article proposes the design, fabrication, and experimental validation of a six-port (6×6) modified planar rectangular MIMO antenna array for mid-band 5G smartphone applications. The proposed array operates over a frequency range of 2.63 GHz to 6.64 GHz, achieving a bandwidth of approximately 85% centered at 4.63 GHz, covering essential sub-6 GHz 5G bands. The array's isolation between ports is primarily maintained below -20 dB, ensuring minimal mutual coupling. The Realized Gain (RG) ranges from 4 to 6 dBi, while the Total Efficiency (TE) reaches up to 80%. Furthermore, the Envelope Correlation Coefficient (ECC) remains as low as 0.002, and the Diversity Gain (DG) is nearly constant at 10 across the operating bandwidth. The Specific Absorption Rate (SAR) values are well below regulatory limits, with the lowest measured at 0.175 W/kg and the highest at 1.27 W/kg, ensuring safe usage for mobile applications.*

Keywords *- MIMO, BW, 5G, RG, TE, ECC.*

1. Introduction

The paradigm of wireless technology is ever-evolving. For the last few decades, the world has seen the evolution of this technology from 0G to 5G and is now eyeing toward beyond 5G. Compared to the limitations of the 4G, this emergence of the 5G technology has brought a lot of benefits. Among them, the prime contribution is the very low latency of only 1 millisecond. This technology's other features are higher data rates, comparatively better connectivity, and throughput [1]. Notably, 5G's ability to function across diverse frequency bands highlights its potential for widespread global adoption. Again, the Multiple Input and Multiple Output (MIMO) system has transformed wireless communication systems with higher signal selectivity, better diversity, beamforming and others. Nowadays, the User Equipment (UEs) such as smartphones/handphones and Base Transceiver Stations (BTS) in mobile communication cannot be developed without the help of this technique and has become an integral part of it.

There are mainly three frequency bands that are utilized by 5G MIMO communication depending on the country/zone of the vendors: (i) the sub 1 GHz bands, (ii) the sub 6 GHz bands and the millimetre wave (mmWave) bands. In Malaysia, some vendors use the 700MHz (sub 1 GHz) band, and others use the 3.5 GHz (sub-6GHz) band. Other countries, such as China, use the two separate bands of 3.3-3.6 GHz and 4.8-5 GHz of the sub-6GHz bands. Some countries in Southeast Asia also use the 4.8-6 GHz band. The mmWave frequencies range from 24 GHz, reaching up to 60 GHz for some Europe and North American standards [2].

Therefore, due to the diverse frequency ranges used by the 5G, the design of the UEs is becoming more challenging day by day. Furthermore, large numbers of vendors using different bands of the sub-6 GHz ranging from 3-6 GHz ask for a wide band of UE operations. One of the key elements of the UEs is the integrated antennas, which are used as the wireless gateway for receiving/transmitting the Uplink/Downlink (UL/DL) signals. Consequently, the challenge falls upon the antenna engineers to design antennas to keep the performance intact for 5G communication. The challenge becomes greater if the MIMO array is designed for smartphones.

As a greater number of Single Element Antennae (SEA) defines the better the performance, the challenge is mainly due to the smaller space inside the case structure of the phone. Additionally, keeping the performance of the other circuitry intact is quite challenging. The MIMO antenna arrays in the

sub-6 GHz ranges can be tuned mainly based on four factors: the working Bandwidth (BW), number of SEA, arrangement of the antenna array on the phone, and the isolation technique. So, constructing a MIMO array for smartphones that can deliver a balanced performance with good isolation features, wider BW of operation, low profile, and a simple structure is necessary. To deliver this by keeping the SEAs as low as possible and other mobile circuitry unharmed is still a huge, challenging job for antenna design engineers.

One of the earliest works is proposed in [3], where a 5G two-element (2×2) reconfigurable MIMO array is proposed. The array has two different working bands: one at 2.4 GHz and the other at 3.5 GHz. In that work, the authors used reconfigurable switches to tune between these two bands to create the frequency diversity. Two meander-lined microstrip patches as the SEAs are used to operate at 2.4 and 3.5 GHz distinctly. The results show that the array has a remarkable ECC of 0.0056 and 0.0009 at both operating frequencies, respectively. Yet, the array suffers from low isolation between the ports, achieving a mere -12dB only, which hinders the performance of the proposed design, and the proposed array is not designed for the mobile phone application. Another dual-band dual-element design has been presented that works at sub-6 GHz and mmWave smartphone applications [4]. The working BW of this array is 3.5-4.3 GHz (at sub-6 GHz) and 24-38 GHz (at mmWave). It is observed that the port isolation of levels of -21dB and -24 dB are attained in the sub-6 and the mmWave 5G bands. The authors have used the specific positioning of the metamaterials between the antenna elements to achieve good isolation. Even though this MIMO has good isolation characteristics, the ECC is high, reaching 0.05 as the highest tolerance is 0.04 for the MIMO standard**,** where the lower value is desirable. Another issue is that no SAR analysis has been presented, which is very important for close-body devices.

In order to extend the MIMO system capacity, the authors in [5] have proposed a four-element (4×4) planar MIMO antenna array working within the sub-6 GHz separate dual-band centred at 3.5 GHz and 4.9 GHz with a 200 MHz working BW for each band. However, its efficiency is limited, reaching only 70% due to moderate isolation (16.5 dB) achieved despite using parasitic rectangle strips. Another approach in [6] leverages the combined techniques called ‘space’ and ‘pattern’ diversity by proposing a four-element array for the 5G handsets. The authors have employed the dipoles for SEA and used four SEA for array design. This design offers dual-band with a dual-diversity feature; however, suffers from relatively low isolation (-15 dB) and limited efficiency (51% at port 1). While the study includes a good SAR analysis with results within safety limits (1.7 W/Kg at 3.5 GHz), further improvements in isolation and efficiency are necessary. Recently, a meticulously designed another 4×4 dual-band MIMO design is proposed to integrate into the 5G mobile devices. This design utilizes an antenna placement technique called side edge positioning. The proposed design operates effectively over two distinct frequency bands. One is centred at 3.5 GHz with 200MHz BW, and another is cantered at 4.9 GHz with same BW. This arrangement secures an isolation level of -17.5 dB which is within the standard range. However, despite of this contribution, the array exhibits an Total antenna Efficiency (TE) of mere 60% and an ECC below 0.05 across both operating frequency bands [7].

Apart from the two- and four-element MIMO array antennas, recently, some proposals have been made for a higher number of SEAs, even reaching up to 12 elements for smartphones. In [8], a 6×6 MIMO (six elements) array is proposed by the authors working from 1.6-2.6 GHz covering the Wi-Fi, LTE and carrier aggregation applications. The design is proposed on the cheap FR-4 substrate with a small final dimension of 39×29 mm2. The design has a good maximum isolation of 45.6 dB. Also, the measured efficiency is as high as 88%. The maximum gain and ECC of 3.34dBi and 0.15 show a decent MIMO performance, respectively. However, from the results, it is realized the isolation between ports 1 and 2 is very poor, only reaching up to 12.5dB, hindering the performance of the design. Also, the overall working BW of the antenna is not similar for all ports of the design, including difficulty with selectivity while operating. Similarly, in [9], it can be seen that there is another proposal made with a 6-port MIMO array antenna for futuristic smartphones. The proposed antenna works from 2.3-6.5GHz, covering the n77-n79 5G bands and the WLAN. The proposed structure is simple and designed on the FR-4 substrate. The isolation performance between ports is $>$ 20 dB, with the ECC value reaching less than 0.01. However, the entire work has been done by simulation, and no experimental validation has been performed. In addition, no SAR results were presented. As the proposed design is for a smartphone application, the SAR analysis is crucial to assess the quality of the design for this specific application.

The authors in [10] have proposed another 8-element MIMO for the 5G mobile communications. The authors utilized the dual-polarized Self-Complementary Antenna (SCA) pair and mounted four of the pairs at the edge corners of the inner board of the phone so they would not affect the phone’s main circuitry. The array works at a 3.6 GHz band. To make them an SCA pair, the antennas are placed in both top and bottom layers at the edge corners of the phone. The main feature of this design is that it can produce a dual-polarized beam. The array achieves a high single-element (IEEE) gain of 4.1dBi. The ECC is very low keeping, always below 0.004 at 3.6GHz. The SAR result reveals that the highest value is 1.8 W/Kg, which is within the standard. However, it is seen that one of the most important performance parameters, isolations between ports 1 and 2, have suffered to go down to less than 12dB. This is undesirable for any MIMO array. One innovative approach has been proposed to estimate the optimal dimension of the

MIMO antenna array with 8-elements [11]. The array works for the sub-6 GHz bands. The authors have utilized the side mounted method to propose the design. While the design achieved a good operating BW of 45% of the centre frequency, it still failed to achieve good isolation, obtaining only a mere -12.5dB. Also, the S11 reference BW is taken as -6dB, which is high.

Similarly, in [12], another 8×8 array has been proposed utilizing the modified ground structure. The proposed design includes an L-shaped top patch with a prob feed technique that covers the 5G NR midbands. The design achieved an exceptionally good ECC of 0.08 and is highly efficient, reaching up to 85%. Furthermore, a detailed SAR analysis has been conducted to prove the compatibility of the design with smartphones. Yet, the same problem persists; the antenna array can only obtain a -11dB isolation between the ports, which is below the MIMO standard value.

Jumping onto a higher number of elements, a 10×10 array has been proposed in [13]. The array works at a centre frequency of 3.7GHz with a BW of 1GHz covering the midband 5G. The proposed array got a good ECC and DG of 0.07 and 9.7, respectively, at the centre frequency. The SAR value is well within the range of 1.28 W/Kg for 1g tissue. However, the antenna suffers from a low efficiency level of 65% only. Furthermore, the isolation is still below the standard level going as low as -11dB. Analogously, the authors in [14, 15] proposed a higher element (12 elements) MIMO array. The first one is for the rimmed smartphone application, and the other is designed as a tri-polarized array for future 5G smartphones. Both placed the antennas at the side edges of the board to improve the isolation between the ports at 3.5GHz. Still, the antenna suffered from low isolation between the ports in both cases. Table 1 summarises the key parameters of this study.

Table 1. Summary of the recent works on MIMO antennas for 5G smartphone

Ref	Technique Used	BW (%)	Isolation (dB)	%TE	ECC	SAR (W/Kg)
[3]	Meander-line	na	-12	65	0.02	Na
[4]	Meta-material	na	-21	50	0.05	Na
[5]	Side edge arranging	87	-17.5	60	0.05	Na
[6]	Parasitic strip	5.7/4	-16.5	70	0.01	Na
[7]	Diversity technique	26.5	-15	51	0.005	1.7
[8]	Parasitic and slotted GP	na	-12	88	0.002	Na
[9]	Slotted Ground	na	-12	70	0.03	Na
[10]	Edge corner feeding	21.6	-12	70	0.004	1.8
[11]	Deep Learning	11.1	-12.5	Na	0.1	Na
[12]	L-slotted GP	na	-11	87	0.08	Na
[13]	Slotted Ground	27	-11	65	0.07	1.28
[14]	Side edge mounting	5.7	-12	39	0.42	Na
[15]	Side edge mounting	5.7	-10	36	0.4	Na
This Work	**PGP**	**85**	**-20**	**80**	**0.002**	**0.175**

To address these aforementioned issues discussed in this article, a half-circular slotted modified rectangular patch 6-element (6×6) MIMO array design. This proposed array has no parasitic or metamaterial element. To improve the BW, the Partial Ground Plane (PGP) technique is used and also, to improve the Port to Port (P2P) isolation, the sequential spatial rotation technique has been utilized. The proposed design is simulated by CST MWS 2022 and has been fabricated and validated on the Rogers 5880 with a dielectric constant (ε_r) of 2.20, height (h) is 0.508 and the tangent loss factor of 0.0009.

2. The SEA and MIMO Design Procedure

Figure 1 shows the design layout of the proposed single and MIMO (6-element) array. Figures 1(a) and 1(b) comprise the simulated layout in CST MWS of the SEA. Also, Figure 1(c) and Figure 1(d) illustrates the fabricated top and bottom view of the SEA on the Rogers 5880 substrate, respectively. Similarly, Figures 1(e) and 1(f) illustrate the simulated layout view of the MIMO array. Furthermore, Figures 1(g) and 1(h) illustrate the fabricated top and bottom view of the MIMO. It is seen in Figure 1(a) that the antenna has a dimension of 42.5×27 mm2.

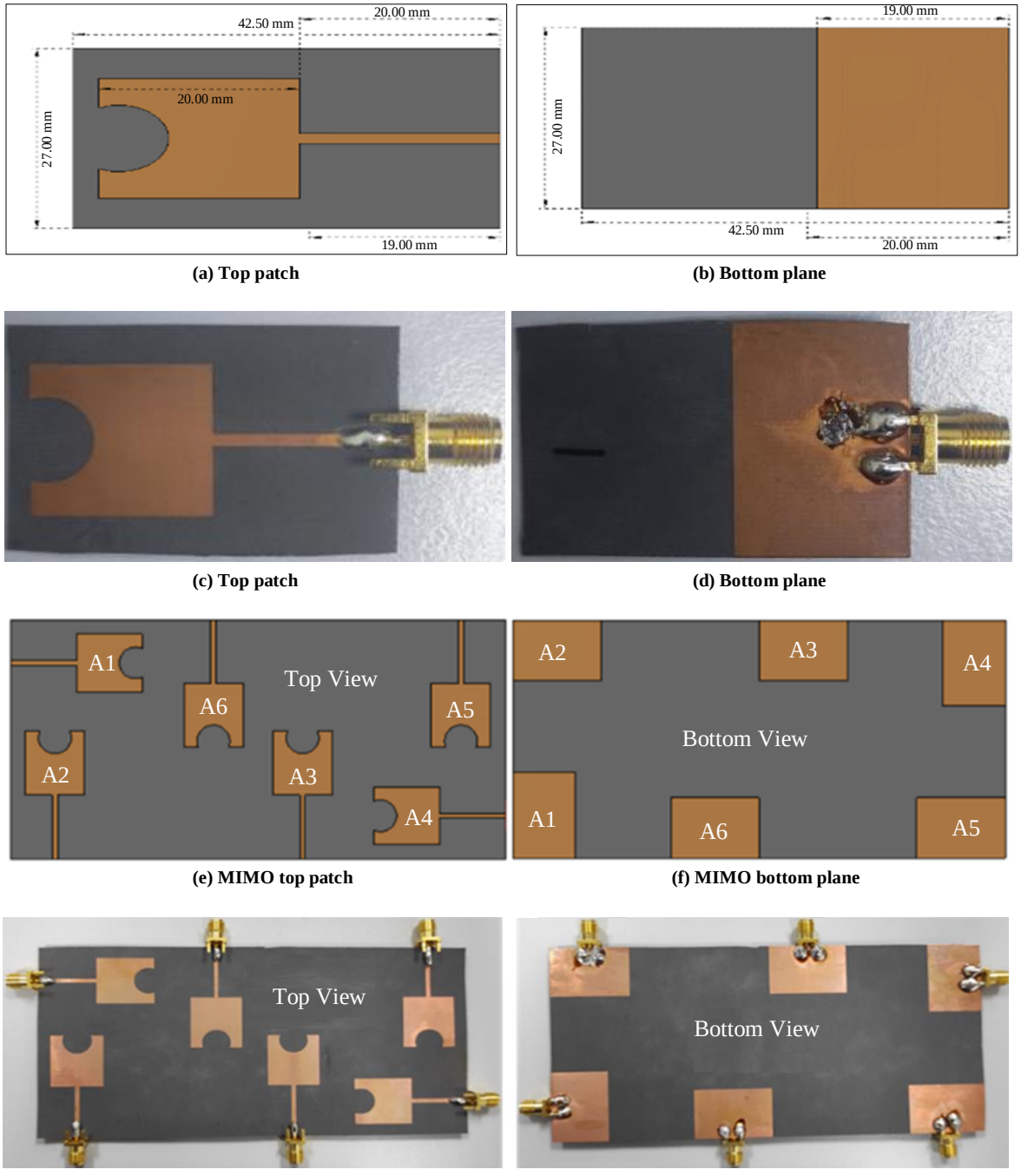

(a) Top patch **(b) Bottom plane**

(c) Top patch **(d) Bottom plane**

(e) MIMO top patch **(f) MIMO bottom plane**

(g) MIMO top patch **(h) MIMO bottom plane**

Fig. 1 SEA simulation and fabrication

It is also observed that it has a top-modified rectangular patch with a half-circular slot inserted into it at the top of the rectangular-shaped patch. The patch is a square with a side of 20 mm and a half circular slot inserted having a radius r = 5mm. The center circular slot is on the midpoint of the top line of the patch. A microstrip feeding technique is used for this design with an optimized length of 20mm. The width is estimated as 1.55mm, representing the 50Ω Transmission Line (TL) on the Rogers 5880 substrate at a center frequency of 4GHz. The Ground Plane (GP) length is truncated to 19mm to create a Partial Ground Plane (PGP) while the width is maintained the same as the width of the antenna [16]. All related dimensions are estimated with the help of Equation (1)-(10) and later optimized using CST MWS 2022. Where (1)-(2) are utilized to approximate the rectangular dimension of the patch, and the total length and width of the antenna are optimized.

$$W_p = \frac{C_0}{2f_c\sqrt{\frac{(\varepsilon_r+1)}{2}}} \quad (1)$$

$$L_p = \frac{C_0}{2f_c\sqrt{\varepsilon_e}} - 0.824h\frac{(\varepsilon_e+0.3)(\frac{W_k}{h}+0.264)}{(\varepsilon_e-0.258)(\frac{W_k}{h}+0.8)} \quad (2)$$

$$r = \frac{F}{\left\{1+\frac{2h}{\pi\varepsilon_r F}\left[ln\left(\frac{\pi F}{2h}\right)+1.7726\right]\right\}^{\frac{1}{2}}} \quad (3)$$

$$F = \frac{8.791\times10^9}{f_c\sqrt{\varepsilon_r}} \quad (4)$$

In addition, the Equation (3) and (4) are used to approximate the radius of the half-circular slot on the patch [3]. Next, it can be seen from Figures 1(e) and 1(f) that the MIMO antenna has been constructed with six different elements with a careful sequential rotation of 90^0. The proposed MIMO array consists of six different elements denoting from A1-A6. The antenna A1 and A2 are 90^0 polarization apart and the same scenario is seen between the antenna A3 and A4. The other two antennas (A5, A6) cannot be rotated 90^0 due to the limitation of the space on the PCB board. So, those antennas are located on the opposite side of the antenna board to evade the interference between them. Antenna A5 and A6 are placed 85mm away from the antenna A3 and A4, respectively. Figures 1 (g) and 1(h) illustrate the proposed array's fabricated top and bottom view. In the next section, the detailed results of the design stages of the SEA, the antenna parameters of both the SEA and MIMO, and the performance parameters of the MIMO and SAR analysis are discussed.

3. Result and Discussion for Validation

Figure 2 comprises the design stages of the proposed SEA for the MIMO and the results associated with it. At stage 1 (Figure 2(a)), it is seen that the antenna is simulated with a rectangular patch of the same area, as stated in Figure 1(a), connected with a microstrip feed with a Full Ground Plane (FGP). The s-parameter (S_{11}) results of all the stages are shown in Figure 2(b).

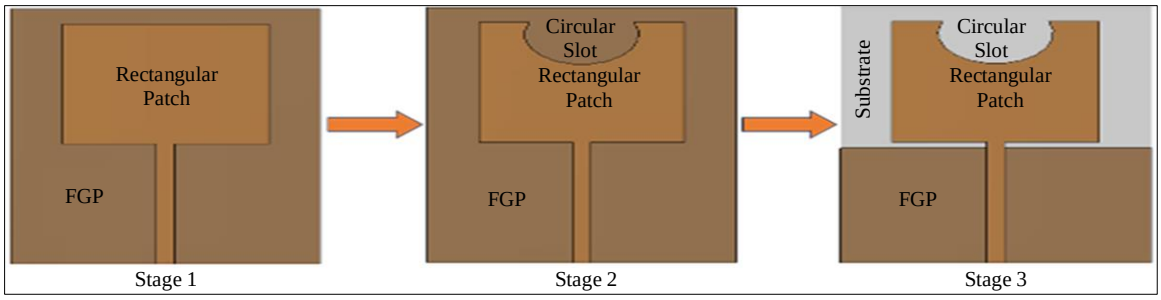

(a) Design stages

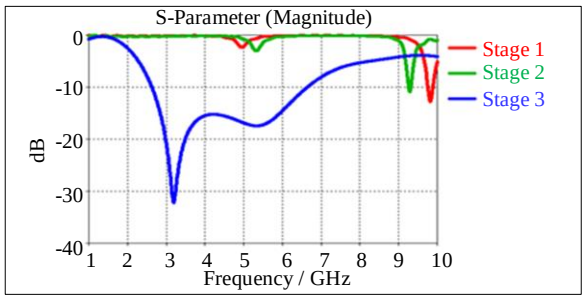

(b) S11 (stage 2)

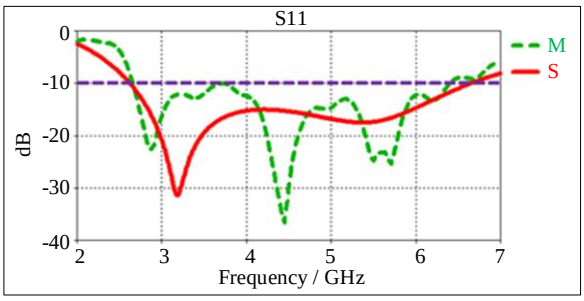

(c) S11 (stage 3)

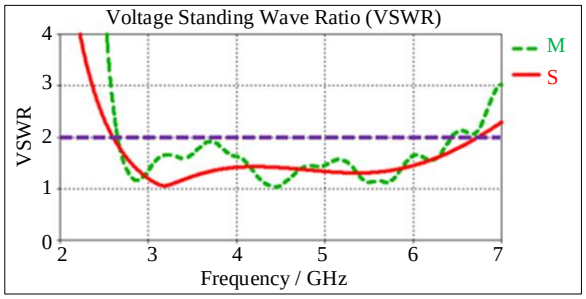

(d) VSWR

Fig. 2 Different stages of the SEA development

Initially, no visible resonance was exhibited in the 5G mid-band range. At 9.8GHz, it can be seen that there is a -10dB resonance; however, that's out of the targeted band. Additionally, there is a small dip (-4dB) in the S11 around 5GHz. Next, stage 2 shows that a circular slot with a radius of 5.2 mm is inserted at the top side of the patch, still with an FGP. As observed in Figure 2(b), there is a change in the S11 response due to the adjustment in stage 2. Still, there is no visible resonance inside the targeted range of frequency. Finally, the full GP is reduced to 19mm to produce a PGP in stage 3. It is seen that there is a remarkable change in the S_{11} response, noticing that the response falls below -10dB, roughly between 2GHz-7GHz. Figure 2(c) comprises the exploded view of the simulated and measured S_{11} for stage 3. The measurement was done by the VNA using Keysight model number N5230A PNA-L. Also, it is seen that the simulated S_{11} response goes below -10dB from 2.63GHz-6.64GHz, making a BW of 4.01GHz which is approximately 86.5% of the center frequency of 4.64GHz.

However, while looking into the measured results, it agrees but with a little difference at the higher frequency side of the BW. A small ripple is visible around -10dB but does not lose any BW. Continuing to validate the working BW of the antenna, Figure 2(d) comprises VSWR responses (simulation and measurement) of the proposed SEA. Similar to the S_{11} response, it is observed that they are in agreement also with a noticeable ripple around 6.3 GHz but still, it can be considered that the BW is intact for operation. So, it can be said that the S_{11} and the VSWR results confirm that the antenna is working well within the targeted 5G mid-band frequencies. Figure 3 comprises some more antenna performance parameters for the proposed SEA design. Figure 3(a) shows the matching of the microstrip feed for this design, and it is observed that the reference impedance is exactly the same as 50Ω. Furthermore, illustrated in Figure 3(b), it is observed that the real and imaginary values of the antenna are 50 Ω and around 0 Ω, respectively, around 3.8GHz, where the matching is the best for this design (around -33dB). This confirms the stability of the design.

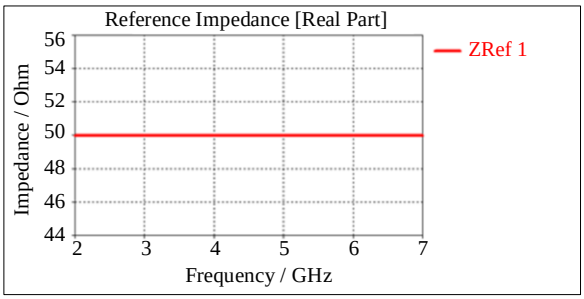

(a) Reference feed impedance

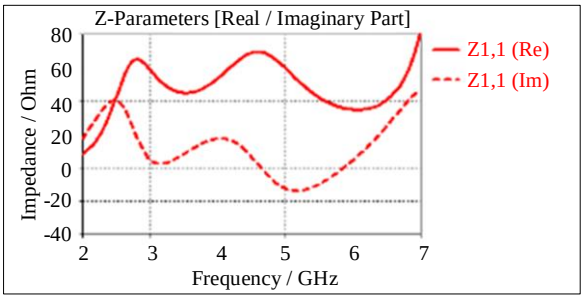

(b) Antenna impedance

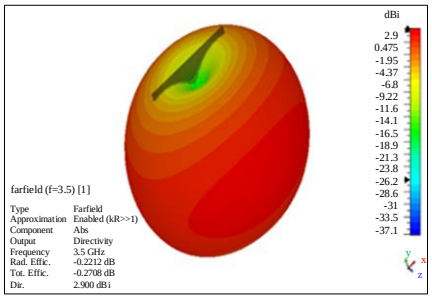

(c) Radiation pattern

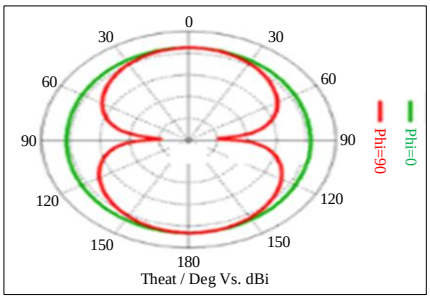

(d) Phi= 00, 900 pattern

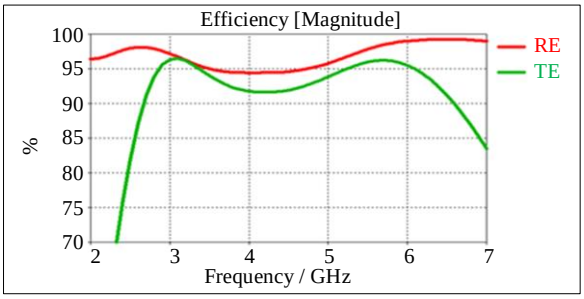

(e) Efficiencies

Fig. 3 Antenna parameter results for SEA

Moreover, Figure 3(c) shows the 3-D pattern of the SEA. It is seen that the pattern is omnidirectional. The 2-D radiation pattern plot is presented in Figure 3(d) to confirm the omnidirectional nature. As expected, it is realized that the phi = 0 plane is fully circular, and the phi = 90 plane is bidirectional, miming the omnidirectional nature. The far-field radiation pattern of the SEA is taken at 3.5GHz. Lastly, Figure 3(e) reveals the simulated Radiation Efficiency (RE) and Total antenna Efficiency (TE). It is seen that the RE stays between 95%-99%, whereas the TE always stays above 92% throughout the entire BW. Moving on to the MIMO design, Figure 4 comprises the setup with VNA (Figures 4(a) & 4(b)) and six different reflection parameter results (simulated and measured) for six different ports. In MIMO systems, isolation separates antenna elements, minimizing signal interference or mutual coupling. High isolation, measured in decibels (dB), ensures minimal power transfer between antennas, improving system performance by maintaining signal integrity, enhancing data rates, and increasing overall efficiency and reliability in wireless communication [17].

(a) Measurement with VNA

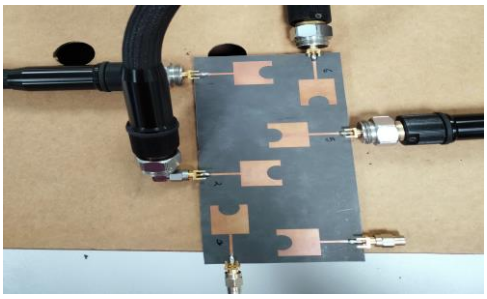

(b) Connection with VNA

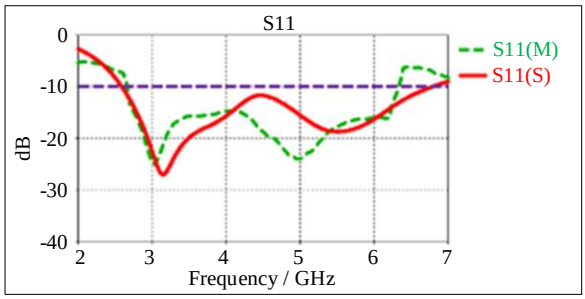

(c) A1

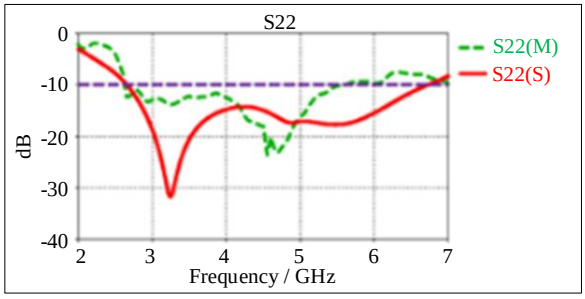

(d) A2

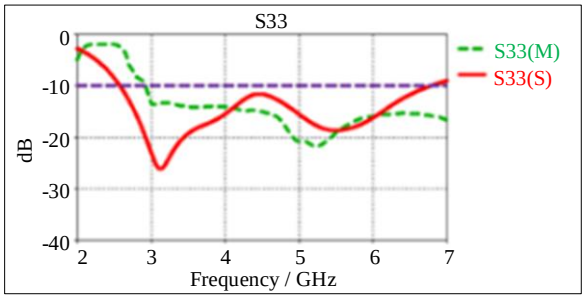

(e) A3

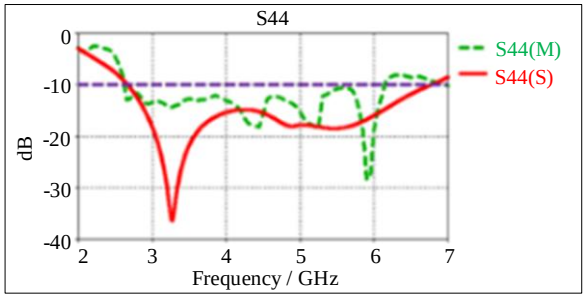

(f) A4

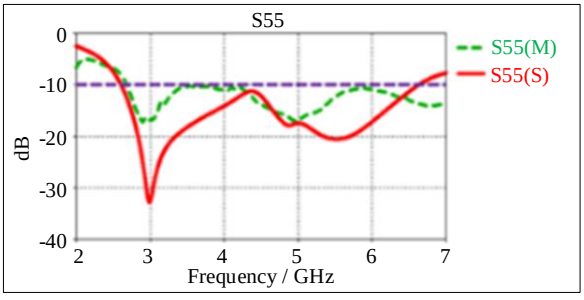

(g) A5

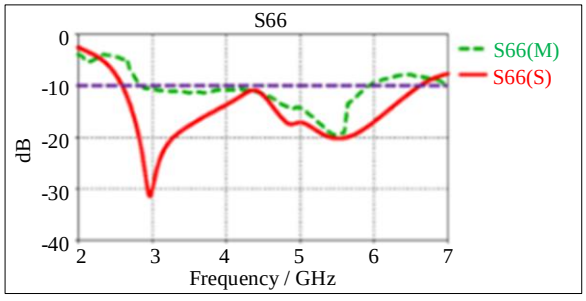

(h) A6

Fig. 4 S11 setup with VNA and results

The reflection parameter is denoted as the Sii where i=1-6 and the transmission coefficient (Sij) of the MIMO array where i≠j (illustrated in Figure 5). In other words, it can also be said that the transmission coefficients are the isolations/mutual coupling between the ports. Figures 4(a) and (b) show that the measurement is done with a 4-port VNA. While measuring 4 ports, the other two unused ports are terminated with 50Ω defined loads. Figures 4(c)-(h) represent the S_{11} results for the A1-A6, respectively. For A1, it is seen that the measurement result has deviated a little bit in comparison to Figure 2. This is possibly due to the change in the substrate dimension and the effect of the mutule coupling. Still, the BW remains almost the same. A similar scenario can also be seen for the other antennas. However, for S_{33} and S_{66}, the BW goes beyond 7 GHz. Nonetheless, if the target BW is achieved, that situation can be ignored. For the isolation results, Figures 5(a), (c) and (e) comprise the simulation and Figures 5(b), (d) and (f) represent the corresponding measurement results.

Figures 5(a) and (b) represent the isolation of port 1 (A1) from other ports. Simulation results show that the lowest isolation at 3 GHz is -20dB (S_{61}). However, it is seen from the measurement that the S_{12} result goes as low as -15 dB between 2.6 GHz – 3.3 GHz. Nevertheless, after 3.3GHz, it increases very significantly, falls beyond -20dB, and remains below that value throughout the BW. The other results in that figure show they are mostly below -30dB, which is an indication of good port isolation. Similarly, Figures 5(c) and (d) comprise the port 2 isolation results with other ports (3, 4, 5, 6). It also includes the isolation results between ports 3 and 4. It is realized that the minimum isolation is -15dB at 3 GHz for S_{52} and S_{62}. As the frequency increases, the value gradually goes down below the -20 dB mark. Remarkably, it is seen from the measured results in Figure 5(d) that all isolation values go below -25dB. So, it can be said that the isolation between port 2 and others is very good, along with port 3 and port 4. Furthermore, the isolation results (measured & simulated) of S35, S36, S45, S46 and S56 are revealed in Figures 5(e) & (f).

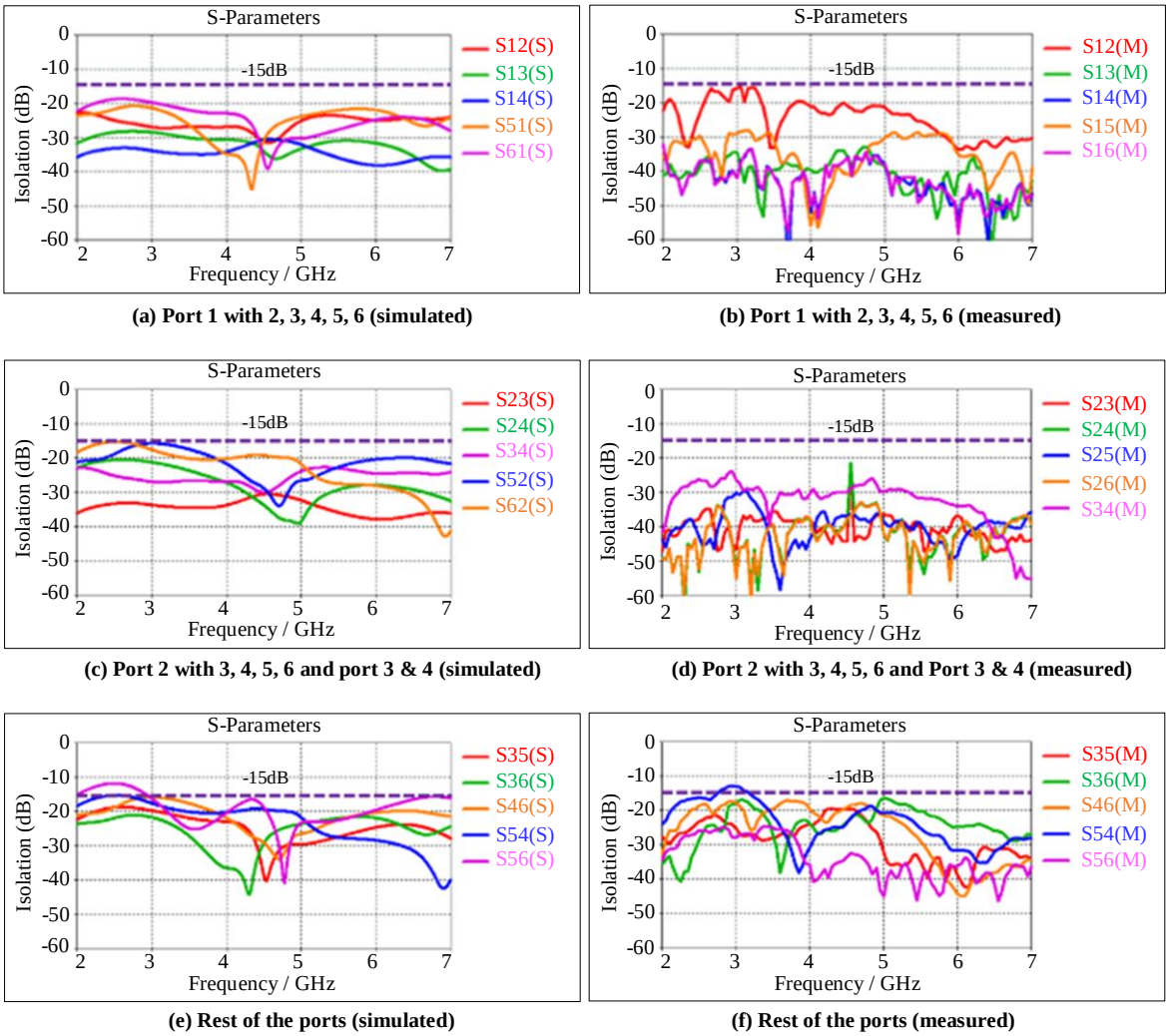

(a) Port 1 with 2, 3, 4, 5, 6 (simulated)

(b) Port 1 with 2, 3, 4, 5, 6 (measured)

(c) Port 2 with 3, 4, 5, 6 and port 3 & 4 (simulated)

(d) Port 2 with 3, 4, 5, 6 and Port 3 & 4 (measured)

(e) Rest of the ports (simulated)

(f) Rest of the ports (measured)

Fig. 5 P2P isolation results

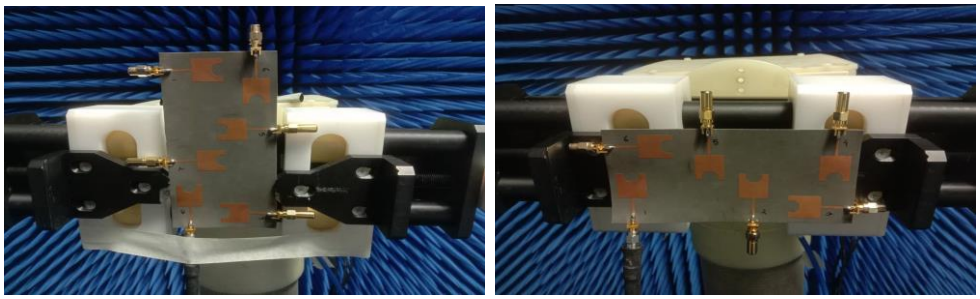

(a) Port 1 measurement (b) Port 2 measurement

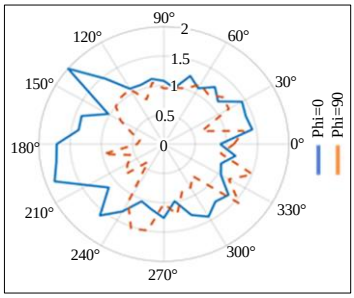

(c) Port 1 2-D pattern

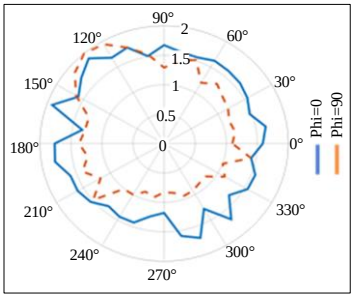

(d) Port 2 2-D pattern

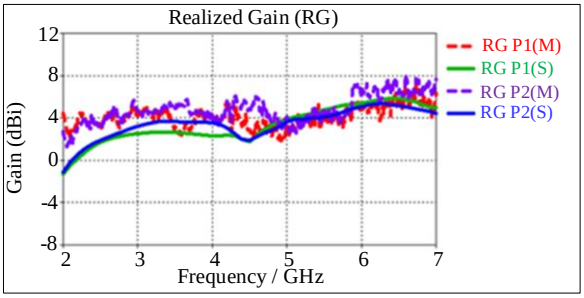

(e) Realized gain

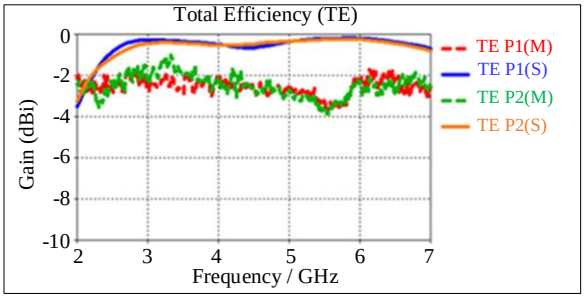

(f) Efficiencies

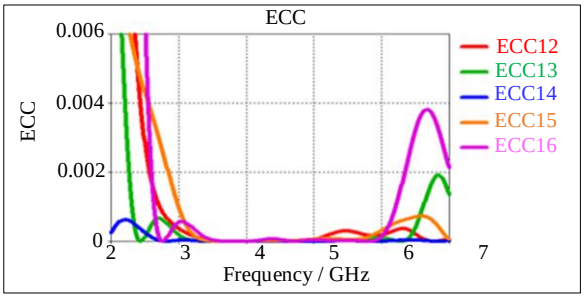

(g) ECC for 6 ports

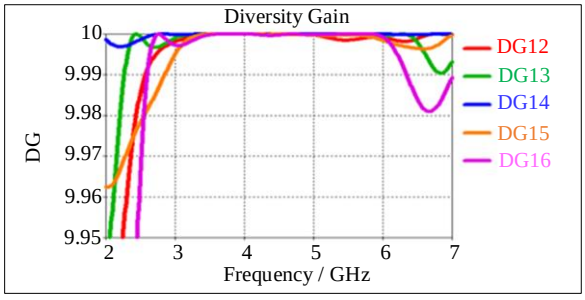

(h) DG for 6 ports

Fig. 6 MINO measurement results

Figure 5 (e) shows the minimum isolation is -15 dB at 3 GHz for S_{56} and S_{46}. The other results are below the -20 dB mark. Moreover, the corresponding measured results also show a very similar pattern. It is seen that at 3.5 GHz, the lowest isolation is -20 dB. However, the isolation result between port 4 and port 6 goes a little low, around 3.8GHz of -17.5dB. Overall, the values are well below the FCC regulation and good to utilize for smartphone purposes. After that, the MIMO antenna array is then evaluated by placing it in an anechoic chamber for the purpose of the measurement of the far-field radiation pattern, Realized Gain (RG), and the TE. The setup and the results are illustrated in Figure 6. For each response only port 1 and port 2 have been considered as the other port resemblances of these two ports. Figures 6(a) and (b) disclose the measurement setup in the chamber. It is seen from the figure that for both measurement cases, the other unused ports are terminated with the 50Ω load.

Figures 6(c) and (d) disclose the 2-D far-field radiation pattern for port 1 and port 2, respectively. At port 1, it is seen that the E-plane (Phi = 0) and the H-plane (Phi = 90) both have a pattern radiating nominally in all directions. A similar scenario can also be seen in Figure 6(d), that both planes at port 2 radiate the same way. This indicates the good radiation characteristic of this proposed design. In Figure 6(e), simulated (S) and measured (M) RG results at ports 1 and 2 are illustrated, and the simulated and measured responses are in good agreement. Mostly, they are between 4-6 dBi values throughout the entire BW, which can be considered a good gain for the low-profile design. Furthermore, Figure 6(f) shows that the measured and the simulated values of the %TE have some differences; however, the pattern is nominally similar. There is a -2dB difference between the measured and the simulated results values.

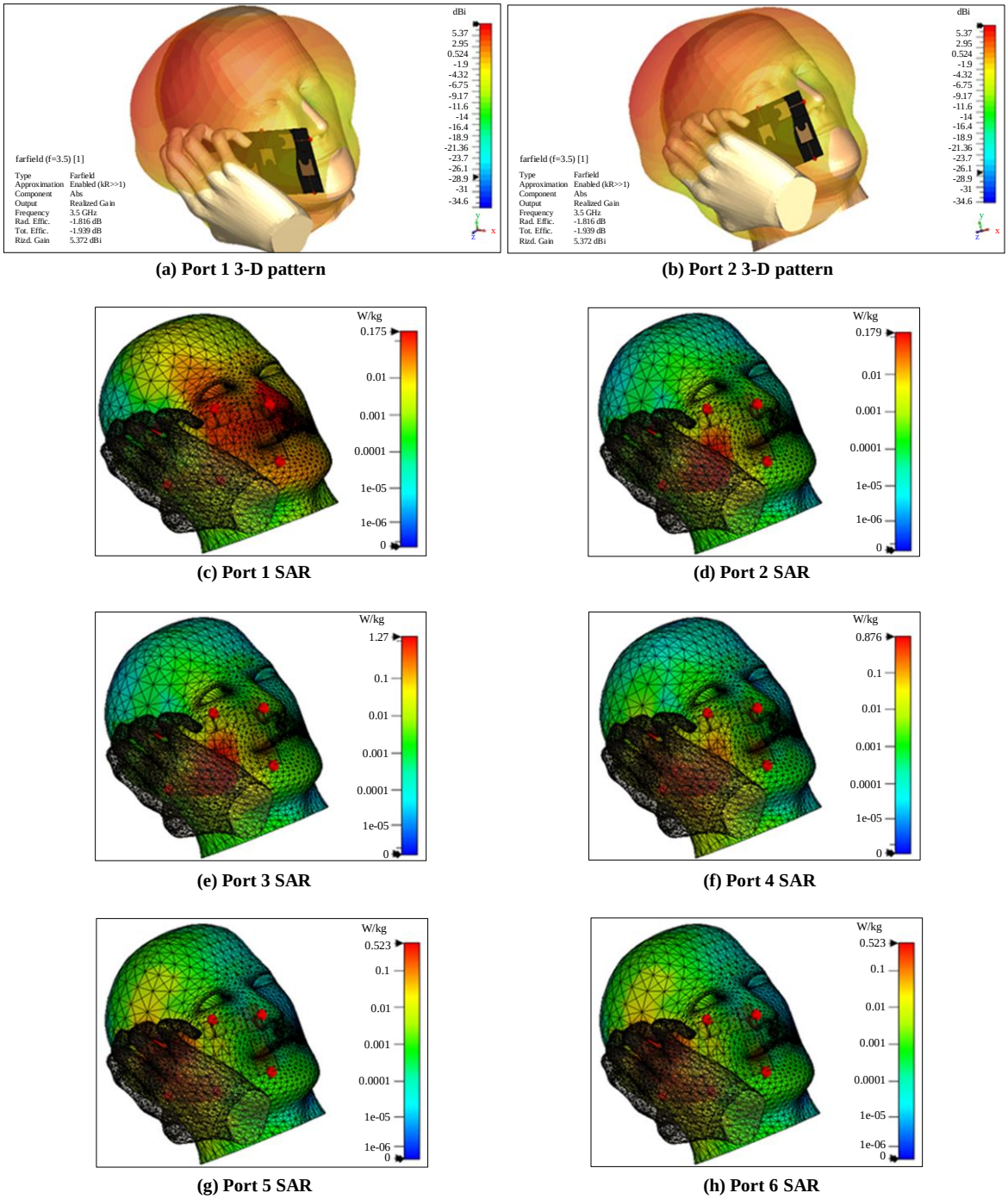

(a) Port 1 3-D pattern

(b) Port 2 3-D pattern

(c) Port 1 SAR

(d) Port 2 SAR

(e) Port 3 SAR

(f) Port 4 SAR

(g) Port 5 SAR

(h) Port 6 SAR

Fig. 7 3-D radiation and SAR results

The simulated results obtained around 0.3 dBm, which represents around 93%, whereas the measured value reached around 80% but fell around 63% around 4GHz. This might be due to the fabrication process and the SMA connector soldering. Nonetheless, the value outruns most of the recently proposed methods. The other important MIMO parameters, the ECC and the DG, are illustrated in Figures 6(e) and 6(f), respectively. In MIMO systems, ECC and DG are essential indicators of system performance. ECC measures the correlation between signals transmitted or received by multiple antennas, with lower values (close to 0) indicating greater signal independence and diversity. A low ECC ensures minimal interference between antenna elements, allowing efficient use of spatial diversity. On the other hand, the DG quantifies the improvement in signal strength and quality due to multiple antenna usage, with higher values (around 10 dB) reflecting better resilience to signal fading. Together, low ECC and high DG improve system reliability and communication efficiency. The ECC and DG standard values are 0.4 and around 10, respectively. Expectedly, it is seen from both ECC and the DG values that they are well within the standard range. The ECC is remarkably low, around 0.002, and the DG is almost 10 throughout the BW. The ECC (ρ) and the DG values are calculated by using the Equations (5) & (6) [18].

Figure 7 discloses the proposed array's radiation and SAR performance in the human hand and head. The SAR measures the rate at which the human body absorbs electromagnetic energy from wireless devices, usually measured in W/Kg. It ensures user safety by regulating RF exposure. SAR limits, set by regulatory bodies, help manufacturers design devices that prevent harmful effects, such as tissue heating, ensuring safe, prolonged device usage. To do so, a hand-head phantom voxel model is defined in the CST MWS to estimate the 3-D far-field (port 1 and port 2 only) and the SAR at all ports. Figures 7 (a) and (b) comprise the 3-D radiation pattern at port 1 and port 2. It is seen in both cases that the pattern is outwards of the hand-head phantom. This means the radiation will not interfere with the head and head much while receiving and sending the signal, which is also good for smartphone applications.

$$\rho_e = \frac{|S_{aa}S_{ab}^* + S_{ba}S_{bb}^*|}{(1-|S_{aa}|^2-|S_{ba}|^2)(1-|S_{bb}|^2-|S_{ab}|^2)} \quad (5)$$

$$DG = \sqrt{1-|\rho_e|^2} \quad (6)$$

Figures 7(c)-7(h) illustrate the SAR setup and the values for port 1 to port 6, respectively. 100mW (20dBm) power is considered in CST MWS while calculating the SAR value for all ports at 3.5GHz. The 10g tissue mass is considered for the calculation where the FCC regulation is < 2.0 W/Kg [19] and desired as low as possible. It is seen that at ports 1 and 2, the values are 0.175 W/Kg and 0.179 W/Kg, respectively, which is remarkably low. Similarly, at port 5 and port 6, a similar value is exhibited, 0.523 W/Kg, which is also very low. Moreover, a slight increase in SAR value is observed at ports 4 and 3, 0.876 W/Kg and 1.27 W/Kg, respectively. Even though the value showed an increase, it was still well below the FCC standard. These results confirm that the proposed antenna array is suitable for smartphone applications in mid-band 5G.

4. Potential Applications and Future Work

The 6-port planar MIMO array, designed for smartphones, has potential applications beyond mobile devices. It can be adapted for IoT devices, enhancing real-time communication and sensor networks. The array could also benefit vehicular communication systems, supporting V2X communications for autonomous driving and traffic management. Future research directions include:

1. Adapting the mmWave 5G communications design to achieve higher data rates and reduced latency.
2. Exploring flexible electronics to develop foldable smartphones and wearable devices.

These advancements require modifying the antenna structure to accommodate shorter wavelengths while maintaining performance. Adapting the design to flexible substrates would contribute to developing more versatile and durable components. By expanding its applications and exploring new technologies, this MIMO array design could solidify its relevance in future communication systems across various industries.

5. Conclusion

A six-port (6×6) planar MIMO array has been designed, fabricated, and validated through experimentation for mid-band 5G smartphone applications. The array works between 2.63GHz-6.64GHz with remarkably 85% BW of the centre frequency of 4.63GHz covering all the mid-band 5G bands. The isolation between the ports is mostly below -20dB within the working BW. The achieved RG is remarkable, going as high as 6dBi, and the TE is as high as 80%. The ECC is outstanding, valued below 0.002, and the DG is almost always 10 throughout the BW. The best feature of this design is the SAR results, dropping as low as 0.175 W/Kg. The future direction of this design is to realize it on the flexible (low profile) substrate that may also be suitable for the folding handset in 5G frequencies.

Acknowledgments

This research is funded by the Fundamental Research Grant Scheme (FRGS) No. Ref: FRGS/1/2022/TK07/UTEM/03/8 and also is conducted in collaboration between Fakulti Teknologi dan Kejeruteraan Elektronik dan Komputer (FTKEK), Universiti Teknikal Malaysia Melaka (UTeM) and faculty of engineering, Internation Islamic University Malaysia (IIUM).

References

[1] Arun Pant, Manish Singh, and Manoj Singh Parihar, "A Frequency Reconfigurable/Switchable MIMO Antenna for LTE and Early 5G Applications," *AEU - International Journal of Electronics and Communications*, vol. 131, 2021. [CrossRef] [Google Scholar] [Publisher Link]

[2] Jingli Guo et al., "Side-Edge Frame Printed Eight-Port Dual-Band Antenna Array for 5G Smartphone Applications," *IEEE Transactions on Antennas and Propagation*, vol. 66, no. 12, pp. 7412-7417, 2018. [CrossRef] [Google Scholar] [Publisher Link]

[3] Abdul Kayum Mohammad Zakir Hossain et al., "A Two-Element Planar Multiple Input Multiple Output Array for Ultra-Wideband Applications," *International Journal of Electrical and Computer Engineering*, vol. 12, no. 6, pp. 6847-6858, 2022. [CrossRef] [Google Scholar] [Publisher Link]

[4] Amany A. Megahed et al., "5G Millimeter Wave Wideband MIMO Antenna Arrays with High Isolation," *EURASIP Journal on Wireless Communications and Networking*, vol. 2023, no. 1, 2023. [CrossRef] [Google Scholar] [Publisher Link]

[5] Jianlin Huang et al., "A Quad-Port Dual-Band MIMO Antenna Array for 5G Smartphone Applications," *Electronics*, vol. 10, no. 5, 2021. [CrossRef] [Google Scholar] [Publisher Link]

[6] Muhammad Ali Jamshed et al., "Dual Band and Dual Diversity Four-Element MIMO Dipole for 5G Handsets," *Sensors*, vol. 21, no. 3, 2021. [CrossRef] [Google Scholar] [Publisher Link]

[7] Zhouyou Ren, and Anping Zhao, "Dual-Band MIMO Antenna with Compact Self-Decoupled Antenna Pairs for 5G Mobile Applications," *IEEE Access*, vol. 7, pp. 82288-82296, 2019. [CrossRef] [Google Scholar] [Publisher Link]

[8] Vandana Yadav et al., "Dual and Wideband 6-Port MIMO Antenna for WiFi, LTE and Carrier Aggregation Systems Applications," *AEU - International Journal of Electronics and Communications*, vol. 162, 2023. [CrossRef] [Google Scholar] [Publisher Link]

[9] Jayshri Kulkarni et al., "Six-Port Symmetrical CPW-Fed MIMO Antenna for Futuristic Smartphone Devices," *2021 6th International Conference for Convergence in Technology (I2CT)*, Maharashtra, India, pp. 1-5, 2021. [CrossRef] [Google Scholar] [Publisher Link]

[10] Naser Ojaroudi Parchin et al., "An Efficient Antenna System with Improved Radiation for Multi-Standard/Multi-Mode 5G Cellular Communications," *Scientific Reports*, vol. 13, no. 1, 2023. [CrossRef] [Google Scholar] [Publisher Link]

[11] Mohamed M. Morsy, "Compact Eight-Element MIMO Antenna Array for Sub 6 GHz Mobile Applications," *SN Applied Sciences*, vol. 5, no. 10, 2023. [CrossRef] [Google Scholar] [Publisher Link]

[12] Zhonggen Wang et al., "Design of MIMO Antenna with Double L-Shaped Structure for 5G NR," *Symmetry*, vol. 15, no. 3, 2023. [CrossRef] [Google Scholar] [Publisher Link]

[13] Muhammad Zahid et al., "Ten-Port MIMO Inverted-F Antenna for LTE Bands 43/48/49 Bands Smartphone Applications," *Electronics*, vol. 12, no. 19, 2023. [CrossRef] [Google Scholar] [Publisher Link]

[14] Chih-Chung Lin et al., "Compact Sub 6 GHz Dual Band Twelve-Element MIMO Antenna for 5G Metal-Rimmed Smartphone Applications," *Micromachines*, vol. 14, no. 7, 2023. [CrossRef] [Google Scholar] [Publisher Link]

[15] Ming-Yang Li et al., "Tri-Polarized 12-Antenna MIMO Array for Future 5G Smartphone Applications," *IEEE Access*, vol. 6, pp. 6160-6170, 2018. [CrossRef] [Google Scholar] [Publisher Link]

[16] Win Adiyansyah Indra et al., "Radio-Frequency Identification (RFID) Item Finder Using Radio Frequency Energy Harvesting," *ARPN Journal of Engineering and Applied Sciences*, vol. 14, no. 20, pp. 3554-3560, 2019. [Google Scholar] [Publisher Link]

[17] Mujeeb Abdullah et al., "High-Performance Multiple-Input Multiple-Output Antenna System for 5G Mobile Terminals," *Electronics*, vol. 8, no. 10, 2019. [CrossRef] [Google Scholar] [Publisher Link]

[18] Mahdi Salehi, and Homayoon Oraizi, "Wideband High Gain Metasurface-Based 4T4R MIMO Antenna with Highly Isolated Ports for Sub-6 GHz 5G Applications," *Scientific Reports*, vol. 14, no. 1, 2024. [CrossRef] [Google Scholar] [Publisher Link]

[19] Rakesh N. Tiwari et al., "A Flexible Dual-Band 4 × 4 MIMO Antenna for 5G mm-wave 28/38 GHz Wearable Applications," *Scientific Reports*, vol. 14, no. 1, 2024. [CrossRef] [Google Scholar] [Publisher Link]